Received 17 December 2018; revised 14 January 2019; accepted 30 January 2019. Date of publication 7 February 2019;
date of current version 1 March 2019. The review of this paper was arranged by Editor K. Shenai.

Digital Object Identifier 10.1109/JEDS.2019.2896971

Counter-Doped Multizone Junction Termination Extension Structures in Vertical GaN Diodes

MOHAMMED SHURRAB (Member, IEEE), AMNA SIDDIQUI (Member, IEEE), AND SHAKTI SINGH (Member, IEEE)

Department of Electrical and Computer Engineering, Khalifa University of Science and Technology, Abu Dhabi 127788, UAE

CORRESPONDING AUTHOR: M. SHURRAB (e-mail: mohammed.shurrab@ku.ac.ae)

This work was supported by Khalifa University Research Fund.

ABSTRACT GaN is an attractive wide bandgap semiconductor for power applications, owing to its superior electrical properties, such as high critical electric field and saturation drift velocity. Recent advancements in developing native GaN substrates has drawn attention toward exploring vertical GaN power diodes with high breakdown voltages (V_{BR}). In practice, effective edge terminations techniques, such as junction termination extension (JTE) structures, play a crucial role in realizing high-voltage devices. Though certain challenges in fabricating GaN diodes, such as difficulty in forming p-type region, makes it difficult to realize edge termination, hence impeding the development and adoption of such devices. This paper aims to address these challenges by presenting the design and methodology of forming multi-zone, counter-doped JTE structures in vertical GaN diodes, which attains close to theoretical breakdown voltage for a wide range of tolerance in implant dose variation. Extensive device simulations using experimental data and including the effects of surface charges and implant profiles, are performed to present realistic results. The results suggest that $>80\%$ of ideal V_{BR} is achievable for a wide range of doping concentration (2.4×10^{17} cm^{-3}) with a maximum V_{BR} reaching 96% of the ideal value. This paper serves as the first step toward leveraging the current challenges in the fabrication of GaN diodes, by proposing optimum design techniques for realizing vertical GaN diodes with high breakdown voltages.

INDEX TERMS GaN, vertical diodes, breakdown voltage, junction edge termination (JTE), counter-doping, partial compensation, multi-zone JTEs (MZJTEs).

I. INTRODUCTION

Gallium Nitride (GaN) based devices are promising candidates for advanced power electronics due to its wide bandgap (3.39 eV), high critical electric field (3-4 MV/s), and high saturation-drift velocity for electrons [1], [2]. The commercially available lateral GaN power devices have shown excellent electrical characteristics [3], [4], however the development of GaN vertical devices is severely hampered by its sensitivity to high defect densities, created by nonnative substrates [5], [6]. The recent developments in native GaN substrates has enabled the exploration and development of vertical GaN power diodes, which have the capability of achieving high breakdown voltages (V_{BR}), high current capacity, better thermal management, with reduced chip area [6]–[9].

Though having a wider bandgap should theoretically lead to high V_{BR}, yet the typical V_{BR} for planar junctions for all wide bandgap semiconductors are far from its theoretical 1-D value. This is primarily attributed to the well-known device edge field crowding caused by three-dimensional junction curvature effects [10]. One way to mitigate the effects of edge field crowding is the use of efficient edge termination techniques, such as junction termination extension (JTE). Effective edge termination structures have been developed for both Si [11]–[13] and SiC [10], however directly transferring these techniques to GaN is difficult due to the processing challenges in GaN. An effective JTE technique requires realization of one or more low doped p-type regions, with the right doping concentration profile.

In GaN, it is difficult to selectively form p-type region, especially low doped p-type regions, by ion implantation or diffusion, due to challenges during processing [4]–[6]. The activation ratio of the implanted dopant ions remains low, and in order to activate the implanted dopants, very high temperatures are required (>1300°C), which leads to the decomposition of GaN [14]. Though recently, an activation ratio of 10% has been demonstrated using novel annealing techniques such as SMRTA (Symmetric Multicycle Rapid Thermal Annealing) [14]. Additionally, various other methods, such as Mg implantation in unintentionally-doped GaN [14], [15] and n-type GaN [16], [17], and selective p-GaN regrowth [18] have successfully shown ways of realizing p-type regions in GaN. However, the latter requires epitaxially growing the p^+ layer using MOCVD, etching outside the main junction, and then regrowing a p-JTE layer, which is a rather complex fabrication process and which may lead to the eventual degradation of material properties. In comparison to p-type implantation, implanting donor ions such as Si, N, etc. and their subsequent activation is much more viable [19]. There have been reports that indicate full compensation of p^+ GaN to create intrinsic insulating layer using nitrogen implantation [6]–[8], as well as lowering the doping concentration of n-GaN layer using Mg ion implantation [20].

Another challenge in realizing an effective JTE design is its sensitivity to doping concentration in the JTE itself. Any slight variations around the desired doping concentration level, a common artifact of the ion implantation process, can lead to considerably lower V_{BR}s. Hence, JTEs should be designed such that high V_{BR}s are achieved, even when there are variations in the doping concentration levels. The viability of single zone JTE (SZJTE) in vertical GaN was studied recently [5], though the device exhibited a breakdown voltage that was considerably lower than expected [6], which can be attributed to the variation in the doping concentration levels in the JTE.

Keeping in mind all the material processing challenges faced by GaN power diodes, it is important that the design of these structures try to compensate for the shortcomings in fabrication, a path also prescribed by the 2018 GaN power electronics roadmap [21]. Hence to overcome the aforementioned challenges, this work, to the best of our knowledge, proposes the first design and methodology of an alternative edge termination technique, where the acceptors in the p^+ layer are partially compensated (counter-doped) by n^+ implantation, to form the p^- JTE region. Moreover, multiple zone JTE (MZJTE) technique is employed, which aims to achieve high V_{BR}, coupled with the insensitivity towards doping concentration variation. The design is developed and verified through simulations by using extensive and realistic material properties (obtained from experimental results) and doping concentration profiles, and accounting for the effects of surface charges. We comprehensively investigate critical design aspects for GaN JTE structures, show optimal design points, and propose the viability of the design by partial compensation using ion implantation.

II. DEVICE STRUCTURE AND SIMULATION SETUP

The device schematic structure of the GaN power diode cell used in this work is illustrated in Fig. 1. The epitaxial structure consists of a 100 μm thick n^+-GaN substrate with a Si concentration of 2×10^{18} cm^{-3}, followed by a 30 μm thick n^--GaN drift layer with a Si concentration of 5×10^{15} cm^{-3} and a 400 nm thick p^+-GaN with Mg concentration of 2×10^{18} cm^{-3}. The main junction of the device, seen towards the left of the device, is made 15 μm wide and an insulating layer on the right has a lateral extent of 15 μm. The JTE, contained in a 400 nm thick layer, is realized by counter-doping the p^+-GaN using n-implantation. To achieve higher percentage of parallel plane blocking voltage and to further mitigate surface electric fields, the JTE total width is made at least three times wider than the drift layer, as will be explained in Section III-A. This makes the overall cell width of the device 120 μm. An ohmic contact (anode) with a thickness of 100 nm and width 10 μm is formed on the p^+-GaN layer and a nitride layer of 100 nm is defined for passivating the surface. Another ohmic contact is formed at the bottom of the device, which acts as the cathode.

Due to the two-dimensional nature of the fields, the best method to optimize the JTE ring design is by computer simulations [22]. 2D device simulator (provided by Synopsys Inc. [23]) is used for all numerical device simulations in this work, with a cylindrical mesh to account for the junction curvature effects. An extensive literature analysis is performed to extract the physical and model parameters for GaN, based on previously verified experimental results. All relevant material and model parameters such as recombination, impact ionization, carrier mobility and lifetime, incomplete ionization, ohmic contacts, etc., obtained from previous experimental results, are used in this work. A partial list of these parameters, at room temperature, is shown in Table 1. The breakdown condition for all simulations is set as the reverse bias voltage at which the impact ionization integral exceeds unity [35].

The impact ionization coefficients (IIC) are the dominant variables in determining the breakdown voltage. The parameters $A_{n/p}$ and $B_{n/p}$ shown in Table 1, are used to obtain a critical electric field of ∼3 MV/cm, which is consistent with the most commonly reported experimental data [3]. The 1D parallel plane theoretical breakdown voltage for the structure is determined to be around 4140 V.

Finally, the design methodology in this work is as follows: - (i) SZJTE simulations with uniform doping concentration profiles are performed to obtain optimum doping concentration where maximum V_{BR} occurs, (ii) desired implant profiles are obtained, based on (i), and tailored using SRIM (Stopping and Range of Ions in Matter) [36], (iii) the implant profiles in (ii) are used to design and optimize the MZJTE structure.

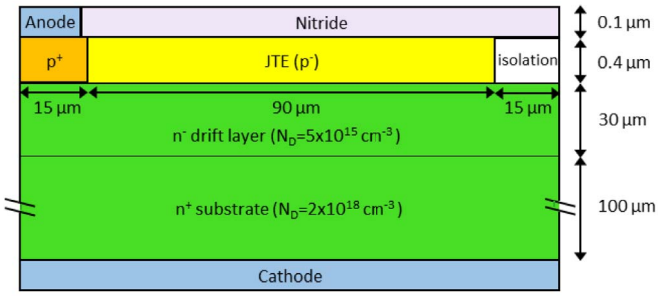

FIGURE 1. Cross-sectional schematic of the vertical GaN power diode cell with a single JTE structure. The JTE is formed outside the main junction by counter-doping the p^+ layer. The structure is terminated by an insulating layer.

TABLE 1. Partial list of GaN material and model parameters (at 300 K).

Parameter name	Value	Ref
Bandgap (Eg)	3.39 eV	[24]
Dielectric constant (ε_r)	8.9	[24]
Electron affinity	4.1 eV	[24]
Effective density of states for electrons	2.3×10^{18} cm^{-3}	[24]
Effective density of states for holes	4.6×10^{19} cm^{-3}	[24]
Effective mass of electrons/holes (m_o)	0.2/1.25	[25][26]
Activation energy for donor/acceptor	17/240 meV	[19][27]
Band degeneracy factor	2	[28]
Electron and hole saturation velocity	$1.27\times10^7/1.7\times10^7$ cm/s	[29][30]
Maximum electron/hole mobilities*	1400/170 cm^2/Vs	[29][31]
Impact ionization coefficients for electrons/holes (A_n/A_p - B_n/B_p)	$1.5\times10^5/6.4\times10^5$ cm^{-1} - $1.41\times10^7/1.46\times10^7$ V/cm	[32]
Auger recombination for electrons/holes	$3\times10^{-31}/3\times10^{-31}$ cm^6/s	[3]
Direct recombination constant	1.1×10^{-10} cm^3/s	[28]
Carrier lifetime of electrons/holes	0.7/2 ns	[3][7]
Critical electric field in this work	3 MV/cm	[32]
Resistivity for contacts on n-/p- GaN	$3\times10^{-6}/4.2\times10^{-3}$ Ωcm^2	[33][34]

*in the analytic mobility model.

III. SZJTE & IMPLANT PROFILE DESIGN

A. SZJTE WITH UNIFORM DOPING PROFILE

Fig. 1 shows the SZJTE structure, where the purpose of a JTE is to allow the spreading of equipotential lines emerging below the junction edge curvature toward the surface [37]. The effectiveness of the JTE lies on the charge available in it. It should be designed such that it is fully depleted at the maximum blocking voltage (optimum charge) and act as a high resistivity layer supporting high fields. If the available charge in the JTE is too low, the extension layer depletes at a much lower voltage, resulting in premature breakdown at the corner of the main junction. Alternatively, if the available charge is too high, the JTE does not fully deplete at breakdown and acts as an extension of the main junction, causing the breakdown to occur at the outermost edge of the JTE, at very low voltages. Hence, it is crucial to control the available charge in the JTE to achieve maximum efficiency.

To achieve higher percentage of parallel plane blocking voltage and to further mitigate surface electric fields, the JTEs total width is usually made at least three times wider than the drift layer. Fig. 2 demonstrates the effect of the width of the JTE on V_{BR}, for a uniform JTE doping concentration of 3.5×10^{17} cm^{-3}. Since V_{BR} saturates when the width reaches 3 × the drift layer thickness, a total width of 90 µm is chosen for the JTE width. Next, the uniform doping concentration profile of the JTE is varied to obtain the highest V_{BR}. Fig. 3 (dashed blue) shows V_{BR} versus the uniform doping concentration of the JTE where the maximum V_{BR} is ∼97% of the ideal value. This corresponds to the full depletion of the JTE at a doping concentration of 3.5×10^{17} cm^{-3}, hence it is the optimal doping concentration of the JTE structure. However, in order to obtain realistic results, the JTE must be simulated as an implant rather than a uniform region. Hence, implant profiles are designed to obtain different desired JTE doping concentration, which is presented next.

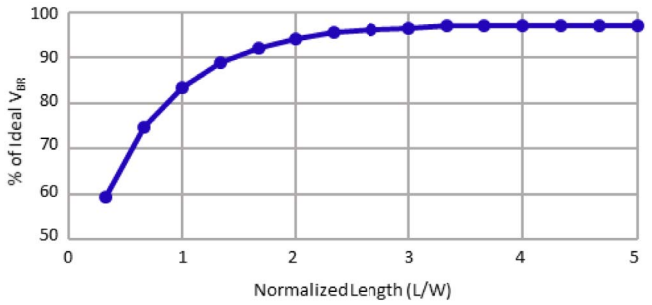

FIGURE 2. Dependence of V_{BR} on the normalized single JTE length with respect to n-drift epilayer thickness.

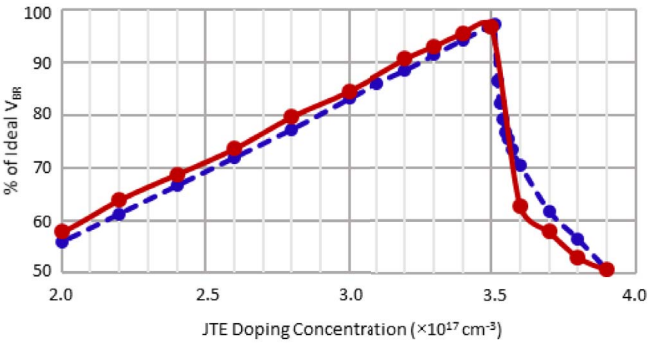

FIGURE 3. V_{BR} vs. JTE doping concentration for uniform doping profiles (dashed) and implant profiles (solid) in SZJTE.

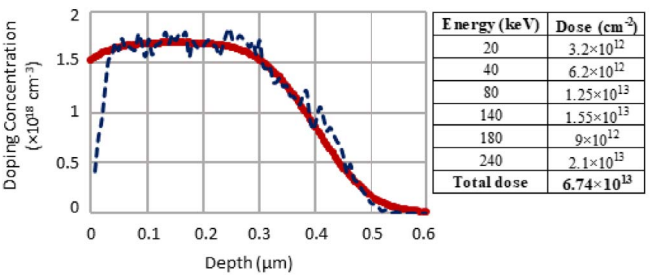

Energy (keV)	Dose (cm^{-2})
20	3.2×10^{12}
40	6.2×10^{12}
80	1.25×10^{13}
140	1.55×10^{13}
180	9×10^{12}
240	2.1×10^{13}
Total dose	6.74×10^{13}

FIGURE 4. n-implant to partially compensate acceptors in p^+ region to produce a JTE doping concentration of 3×10^{17} cm^{-3} simulated in SRIM (dotted) and modeled in the simulations (solid).

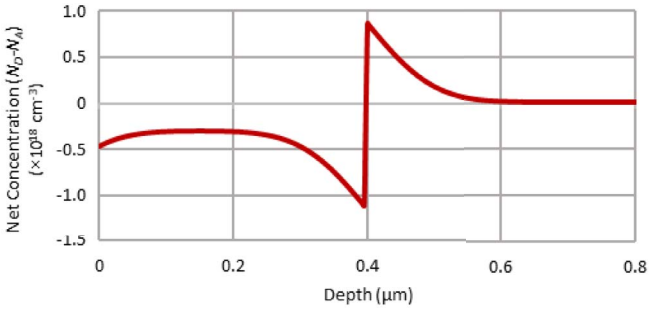

FIGURE 5. The net doping concentration profile in the device after n-type implantation of the profile illustrated in Fig. 4.

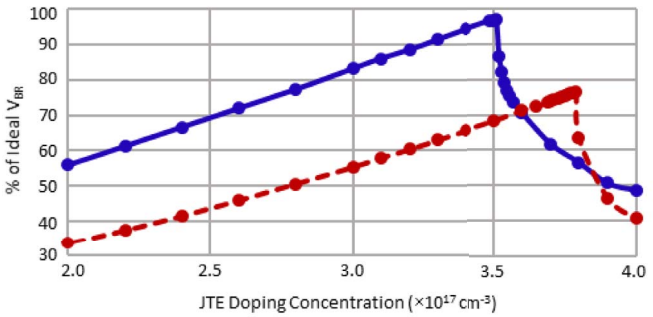

FIGURE 6. Single JTE structure V_{BR} vs. JTE doping concentration for the two different IICs that result in a critical electric field of 3 MV/cm (solid) and 3.75 MV/cm (dashed).

B. IMPLANT PROFILE DESIGN

In order to realize the lightly doped p^- JTE rings in GaN, n-type implantation is used to partially compensate the acceptors in the heavily doped p^+ layer. For any p^- JTE doping concentration, the total dose of the n-implant can be determined using Eq. (1)

$$n\text{-}implantdose = \left(N_{A(Epi)} - N_{A(Desired)}\right) \times T \qquad (1)$$

where $N_{A(Epi)}$ is the doping concentration of the p^+ layer, $N_{A(Desired)}$ is the desired JTE ring doping concentration, and T is the thickness of the JTE ring. For example, for a structure with p^+ epilayer doping concentration and thickness of 2×10^{18} cm^{-3} and 0.4 μm, if the desired JTE doping concentration is 3×10^{17} cm^{-3}, then a donor concentration of 1.7×10^{18} cm^{-3} (corresponding to an n-type dose of 6.8×10^{13} cm^{-2}) is required.

SRIM is used to obtain desired implant profiles, by varying dose and energy. These profiles are then fitted using a Gaussian profile in the device simulator, where the effect of lateral and longitudinal straggle (obtained from SRIM) is also considered. The profiles, to define a range of desired doping concentration levels, are obtained by scaling the dose of a single implant profile in the device simulator by using Eq. (1).

The profiles are tailored such that the total implanted donor concentration partially compensates the acceptors in the p^+ layer to a depth of 0.4 μm, thus creating a lightly doped JTE ring. However, it is seen that the expected V_{BR} for such profile, based on the uniform SZJTE simulations, is severely reduced. The tail created by the implant profile increases the donor concentration in the drift layer right under the JTE, creating a thin and highly doped n^+ layer which causes degradation in V_{BR}. If this n^+ layer is too large, the device breakdowns prematurely at the edge of main junction due to high electric fields. This can be prevented to a large extent by lowering the depth of the near constant concentration region of the implant, which also considerably reduces the penetration of the tail in the drift region. This can be achieved by lowering the energy of the last implant cycle. Although the unintended consequence of this is an increase in the acceptor charge in the JTE region. Since JTE is charge dependent, this again leads to a change in V_{BR}. Hence, it is crucial to have a balance between the desired doping concentration profile and its tail. Keeping this tradeoff in mind, the implant profile obtained from SRIM (and its fit) is tailored such that it gives the same results (V_{BR}) as uniformly doped JTE. This is achieved by balancing the depth of the near constant concentration region of the profile with the extent of tail in the drift layer. Subsequently, the Gaussian dose is varied, using Eq. (1), to obtain implant profiles for different doping concentration levels. These implant results are then compared with the uniform JTE results to ensure that they are similar. As an example, Fig. 4 shows one such profile (for a required JTE doping concentration of 3×10^{17} cm^{-3}), where the SRIM profile and its Gaussian fit is displayed. Here, the total dose used is 6.74×10^{13} cm^{-2} to obtain a total donor concentration of 1.7×10^{18} cm^{-3}. Fig. 5 shows the net doping concentration profile ($N_D - N_A$), which is obtained using the implant in Fig. 4 (accounting for the background concentration of 2×10^{18} cm^{-3} in the p^+ region). It is seen that the implant produces a near constant concentration till a depth of ~0.3 μm which creates a short tail in the drift layer.

Fig. 3 shows a comparison between the results obtained from the uniform doping concentration and implant profiles for a SZJTE structure. The results indicate that the desired implant profiles achieve similar V_{BR}s as compared to the uniform profiles for SZJTE. Thus, the obtained desired implant profiles are used in all subsequent simulations.

C. IMPACT IONIZATION COEFFICIENTS

To investigate the effect of electric field on V_{BR}, two different sets of values for IIC are used for an SZJTE structure. Apart from the values listed in Table 1, which gives an electric field of ~3 MV/cm, another set of values for the same parameters ($A_{n/p} = 3.1 \times 10^7$ cm^{-1} and $B_{n/p} = 3.5 \times 10^7$ V/cm), which demonstrate an electric field of ~3.75 MV/cm, is used [6]. These parameters give a theoretical breakdown voltage of 6790 V for the structure in Fig. 1. The V_{BR} comparison between the two electric fields is shown in Fig. 6. For IIC which gives critical electric field of ~3 MV/cm, the efficiency of the JTE is around 97% of the ideal value, achievable at a single doping concentration. However, if the

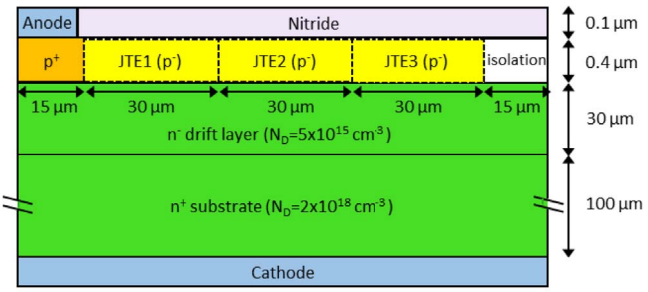

FIGURE 7. Cross-sectional schematic of the MZJTE structure cell. The JTE rings are formed by counter-doping the p^+ layer outside the main junction.

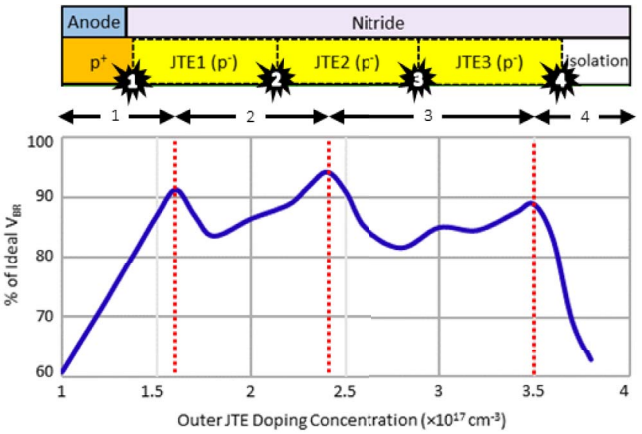

FIGURE 8. V_{BR} as a function of outer JTE doping concentration for a MZJTE structure for $R = (1.5, 1.5)$, used to illustrate the design methodology for MZJTE.

JTE doping concentration turns out to be even 5% higher than the optimal doping concentration, the V_{BR} reduces by ∼30%. For IIC which gives critical electric fields of ∼ 3.75 MV/cm, the maximum achieved V_{BR} is around 75% of the planar ideal value, also at a single doping concentration. The figures indicate that as the critical electric field increases, it is harder to achieve the planar ideal breakdown voltage with a SZJTE structure. This is important as with improvement in GaN material quality, the critical electric field is bound to improve, where recently a critical electric field up to 4 MV/cm was obtained [9], thus making SZJTE structures unviable.

Also, both curves indicate that for a SZJTE structure, if there is a slight variation in the JTE doping concentration, a common occurrence in an ion implantation process, the V_{BR} varies substantially. Moreover, as discussed in Section III-B, the variations in the tail of the implant profile has a direct effect on the obtained V_{BR}. Hence, to circumvent these issues, a MZJTE structure design is proposed in the next section.

IV. MZJTE DESIGN

Fig. 7 shows the proposed MZJTE structure, containing three JTE concentric rings (as shown by dashed lines) around the main junction – inner ring as JTE_1, middle ring as JTE_2, and outer ring as JTE_3. The total width of the three JTEs is designed to have the same footprint (90 µm) as that of SZJTE structure to maximize V_{BR}. The doping concentration of each JTE ring must be low enough such that it is fully depleted before avalanche breakdown occurs [22], and it should decrease in each subsequent ring while moving away from the main junction. Hence, it is helpful to adopt a systematic method of specifying the optimized doping concentration in each JTE ring. One approach is to change the doping concentration between the JTE rings by making use of doping ratios. Hence, for all subsequent simulations, the variables that are optimized are–

1) The doping concentration of the outer ring, i.e., JTE_3.
2) Outer ratio (r_o): The ratio of the middle ring's doping concentration to the outer ring's doping concentration; i.e., $r_o = N_{A(JTE2)} : N_{A(JTE3)}$.
3) Inner ratio (r_i): The ratio of the inner ring's doping concentration to the middle ring's doping concentration; i.e., $r_i = N_{A(JTE1)} : N_{A(JTE2)}$.
4) Pair of ratios (R): An ordered pair of the inner ratio and the outer ratio respectively; i.e., $R = (r_i, r_o)$.

As an example, to illustrate the use of ratios, for $R = (1.2, 1.5)$ if the outer ring doping concentration is 2×10^{17} cm^{-3}, the corresponding middle ring doping concentration is 3×10^{17} cm^{-3}, while the inner ring doping concentration is 3.6×10^{17} cm^{-3}.

A. DESIGN CRITERIA AND METHODOLOGY

The three JTE rings fully deplete when their respective doping concentration is equal to the optimal doping concentration obtained in Section III-A. The design methodology behind MZJTE and the importance of ratios are explained with the aid of Fig. 8, which shows the breakdown points within the structure with respect to the doping concentration of the outer ring, for $R = (1.5, 1.5)$. The V_{BR} exhibits three peaks as a function of outer ring doping concentration, which correspond to the full depletion of the corresponding ring. The outer ring V_{BR} peak always occurs when its doping concentration is equal to the optimal doping concentration irrespective of R. The V_{BR} peaks created by the depletion of middle and inner rings, with respect to outer ring doping concentration, are determined by r_o and r_i respectively. These ratios are important because, if the values of r_o and r_i are too small, the JTE rings doping concentration will be very close to one another and the structure will behave as a SZJTE structure. On the other hand, for large values of r_o and r_i, the doping concentration of the inner and middle JTEs may become larger than the doping concentration of the main junction. These constraints are used to obtain the limits for both r_o and r_i, where both these ratios should lie between 1.1 and 2. Furthermore, the three V_{BR} peaks should be far enough from one another to widen the desired range of outer doping concentration, while avoiding the valleys

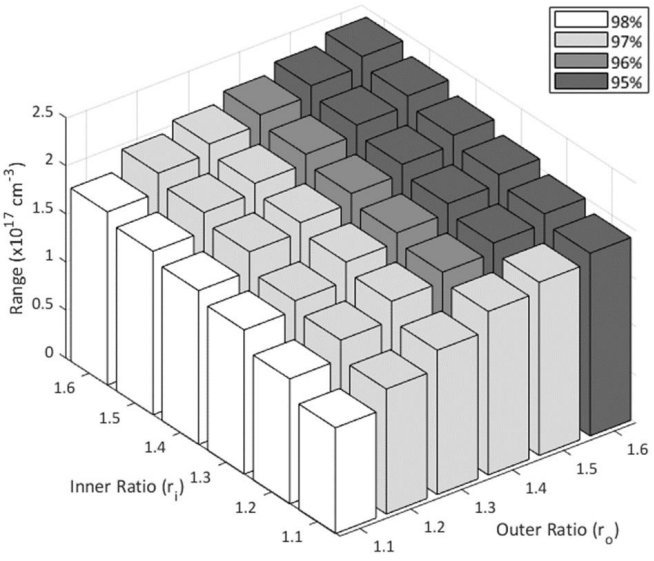

FIGURE 9. Pairs of feasible outer and inner ratios (r_o and r_i) that achieve at least 80% V_{BR} and their corresponding range, while the shade represents the maximum V_{BR} achieved by each pair. As the ratios increase, the range of doping concentration that achieves an acceptable V_{BR} increases, but at the cost of maximum achievable V_{BR}.

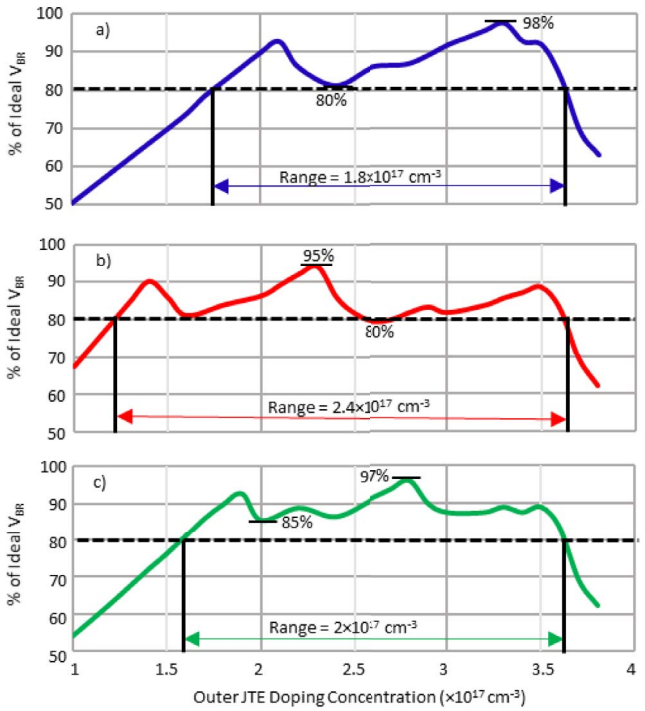

FIGURE 10. V_{BR} vs outer ring doping concentration for three different pairs of R; (a) $R_1 = (1.6, 1.1)$, (b) $R_2 = (1.6, 1.6)$ and (c) $R_3 = (1.5, 1.3)$. The range signifies the doping concentration range which produces at least 80% of the ideal V_{BR}.

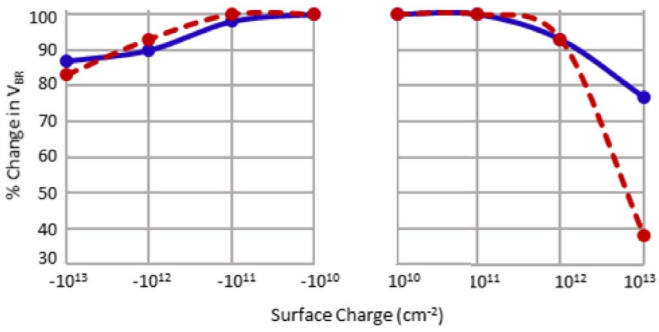

FIGURE 11. The effect of negative and positive surface charges on the V_{BR} of the SZJTE (dashed) and MZJTE (solid) structures. Fixed charges between (-10^{10} and 10^{10} cm^{-2}) do not have an effect on the V_{BR}.

formed in between, which can drop the V_{BR} value to less than the acceptable value, i.e., 80% of the ideal value.

To gauge the performance of the MZJTE, the following metric is used – the design should achieve V_{BR} of at least 80% of the planar ideal value and maintain it over a wide range of outer ring doping concentration (at least 2×10^{17} cm^{-3}). Any pair of ratios R that violates this requirement is not considered in this work.

B. MZJTE DESIGN AND OPTIMIZATION

Since the limits imposed on the ratios are 1.1 and 2, as discussed in Section IV-A, a number of ratio combinations which fall between these limits are considered for subsequent simulations. Fig. 9 shows the different feasible combinations of R that give a range of outer doping concentration with an acceptable value for V_{BR}. Each bar represents a pair of ratios R, where it varies from 1.1 to 1.6. Any values larger than 1.6 cause the valleys between the peaks to drop the V_{BR} value below the 80% threshold, hence are not depicted. In the figure, the height of the bar corresponds to the total range of the outer ring doping concentration, while its shade indicates the maximum achievable V_{BR} for the corresponding pair of R. It can be seen that as both r_o and r_i increase, the desired range of doping concentration increases, but the maximum achievable V_{BR} decreases, which is expected since the higher the ratio, the further the maximum V_{BR} peaks are from one another. For small values of R, the maximum V_{BR} peaks are closer to one another, thus increasing the highest achievable V_{BR}, but for smaller range of outer ring doping concentration. Fig. 10 displays this tradeoff by showing two extremes – $R_1 = (1.6, 1.1)$ for maximum V_{BR} and $R_2 = (1.6, 1.6)$ for maximum range. The pair R_1 achieves a total range of 1.8×10^{17} cm^{-3} with maximum V_{BR} of ~98%, whereas the pair R_2 gives a total range of 2.4×10^{17} cm^{-3} and the highest achievable V_{BR} of ~95%. For the latter, a ~33.3% increase in range only drops the maximum V_{BR} by ~3%. Another pair of ratios, $R_3 = (1.5, 1.3)$, that balances between the range and maximum V_{BR} is also shown in Fig. 10, where the total range of doping concentration is 2×10^{17} cm^{-3} and the maximum V_{BR} is ~97%. Finally, MZJTE results are also confirmed with the uniform results, similar to the SZJTE design discussed in Section III-A.

Overall, the proposed methodology presents various pairs of ratios, as evident from Fig. 9, which can be used to produce MZJTE structures with high range of doping

concentration variation and high breakdown voltages. The designer, therefore, may select a suitable pair of R, depending on the feasibility and the requirements of his or her design.

V. EFFECT OF SURFACE CHARGE

The sensitivity of the JTE structure to surface charge is a reliability issue, as the JTE relies on the control of the implanted charge. Any additional charge on the surface will affect the V_{BR} of the device, since it will alter the charge profile in the JTE. Due to subsequent anneals to activate dopants, the surface is often damaged or morphologically altered, producing unintended surface charges. The effect of both positive and negative surface charge is shown in Fig. 11, for both SZJTE and MZJTE structures. It can be seen that negative surface charge has no significant effect on the JTE effectiveness. However, positive surface charge has no significant effect on the JTE effectiveness until it exceeds $\sim 1 \times 10^{12}$ Scm^{-2} and $\sim 1 \times 10^{13}$ cm^{-3} for SZJTE and MZJTE structures respectively. The presence of negative surface charges helps depleting the n-drift by compensating the positive charge at the ionized donors. On the other hand, the positive surface charge has the opposite effect which enhances the junction curvature and electric field, hence reducing V_{BR}, which is expected for a p-type JTE/n-type substrate [35].

VI. CONCLUSION

In this work, junction termination extension structures for vertical GaN power diodes have been investigated, using calibrated numerical simulations, realistic material parameters, and well-formed design strategy. The advancement of GaN material quality and the invariability of the ion implantation process, makes it difficult to obtain high breakdown voltages with only a single zone JTE structure. Hence, this work proposed the design of MZJTE structures in GaN, where the JTEs are realized by partial compensation of p^+ region, using n-implantation. The results show that by employing the proposed design, breakdown voltages as high as 96% of the ideal value can be achieved for a wide range of doping concentration (2.4×10^{17} cm^{-3}). While further improvements in the fabrication and activation of dopants in the p-GaN will enable the implementation of various edge termination methods to achieve near ideal breakdown voltage, this work aims to contribute towards the advancement in GaN power devices by leveraging the fabrication shortcomings with a comprehensive design for high blocking voltage structures in GaN.

REFERENCES

[1] J. Millán, P. Godignon, X. Perpiña, A. Pérez-Tomás, and J. Rebollo, "A survey of wide bandgap power semiconductor devices," *IEEE Trans. Power Electron.*, vol. 29, no. 5, pp. 2155–2163, May 2014.

[2] E. A. Jones, F. F. Wang, and D. Costinett, "Review of commercial GaN power devices and GaN-based converter design challenges," *IEEE J. Emerg. Sel. Topics Power Electron.*, vol. 4, no. 3, pp. 707–719, Sep. 2016.

[3] G. Sabui, P. J. Parbrook, M. Arredondo-Arechavala, and Z. Shen, "Modeling and simulation of bulk gallium nitride power semiconductor devices," *AIP Adv.*, vol. 6, no. 5, 2016, Art. no. 055006.

[4] J. Hu *et al.*, "Materials and processing issues in vertical GaN power electronics," *Mater. Sci. Semicond. Process.*, vol. 78, pp. 75–84, May 2018.

[5] J. J. Wierer *et al.*, "Simulations of junction termination extensions in vertical GaN power diodes," *IEEE Trans. Electron Devices*, vol. 64, no. 5, pp. 2291–2297, May 2017.

[6] J. R. Dickerson *et al.*, "Vertical GaN power diodes with a bilayer edge termination," *IEEE Trans. Electron Devices*, vol. 63, no. 1, pp. 419–425, Jan. 2016.

[7] I. C. Kizilyalli, A. P. Edwards, O. Aktas, T. Prunty, and D. Bour, "Vertical power p-n diodes based on bulk GaN," *IEEE Trans. Electron Devices*, vol. 62, no. 2, pp. 414–422, Feb. 2015.

[8] J. Wang *et al.*, "High voltage vertical p-n diodes with ion-implanted edge termination and sputtered SiN_X passivation on GaN substrates," in *Proc. IEEE Int. Electron Devices Meeting (IEDM)*, 2017, pp. 9.6.1–9.6.4.

[9] A. M. Armstrong *et al.*, "High voltage and high current density vertical GaN power diodes," *Electron. Lett.*, vol. 52, no. 13, pp. 1170–1171, Jun. 2016.

[10] D. C. Sheridan, G. Niu, and J. D. Cressler, "Design of single and multiple zone junction termination extension structures for SiC power devices," *Solid-State Electron.*, vol. 45, no. 9, pp. 1659–1664, 2001.

[11] V. A. K. Temple and W. Tantraporn, "Junction termination extension for near-ideal breakdown voltage in p-n junctions," *IEEE Trans. Electron Devices*, vol. 33, no. 10, pp. 1601–1608, Oct. 1986.

[12] W. Tantraporn and V. A. K. Temple, "Multiple-zone single-mask junction termination extension—A high-yield near-ideal breakdown voltage technology," *IEEE Trans. Electron Devices*, vol. ED-34, no. 10, pp. 2200–2210, Oct. 1987.

[13] R. Stengl, U. Gosele, C. Fellinger, M. Beyer, and S. Walesch, "Variation of lateral doping as a field terminator for high-voltage power devices," *IEEE Trans. Electron Devices*, vol. ED-33, no. 3, pp. 426–428, Mar. 1986.

[14] T. Anderson *et al.*, "Improvements in the annealing of Mg ion implanted GaN and related devices," *IEEE Trans. Semicond. Manuf.*, vol. 29, no. 4, pp. 343–348, Nov. 2016.

[15] A. D. Koehler *et al.*, "Vertical GaN junction barrier Schottky diodes," *ECS J. Solid-State Sci. Technol.*, vol. 6, no. 1, pp. Q10–Q12, 2016.

[16] Y. Zhang *et al.*, "Vertical GaN junction barrier Schottky rectifiers by selective ion implantation," *IEEE Electron Device Lett.*, vol. 38, no. 8, pp. 1097–1100, Aug. 2017.

[17] T. Oikawa, Y. Saijo, S. Kato, T. Mishima, and T. Nakamura, "Formation of definite GaN p–n junction by Mg-ion implantation to n-GaN epitaxial layers grown on a high-quality free-standing GaN substrate," *Nucl. Instrum. Methods Phys. Res. B Beam Interact. Mater. Atoms*, vol. 365, pp. 168–170, Dec. 2015.

[18] G. Koblmüller, R. Chu, A. Raman, U. Mishra, and J. Speck, "High-temperature molecular beam epitaxial growth of AlGaN/GaN on GaN templates with reduced interface impurity levels," *J. Appl. Phys.*, vol. 107, no. 4, 2010, Art. no. 043527.

[19] W. Götz *et al.*, "Activation energies of Si donors in GaN," *Appl. Phys. Lett.*, vol. 68, no. 22, pp. 3144–3146, 1996.

[20] M. Akazawa, N. Yokota, and K. Uetake, "Detection of deep-level defects and reduced carrier concentration in Mg-ion-implanted GaN before high-temperature annealing," *AIP Adv.*, vol. 8, no. 2, 2018, Art. no. 025310.

[21] H. Amano, "The 2018 GaN power electronics roadmap," *J. Phys. D Appl. Phys.*, vol. 51, no. 16, 2018, Art. no. 163001.

[22] T. Kimoto and J. Cooper, *Fundamentals of Silicon Carbide Technology: Growth, Characterization, Devices*. Singapore: Wiley, 2014, pp. 427–429.

[23] *MEDICI—Two-Dimensional Device Simulation Program User Manual*, 9th ed. Sunnyvale, CA, USA: Synopsys Inc., 2011.

[24] M. E. Levinshteĭn, S. L. Rumyantsev, and M. Shur, *Properties of Advanced Semiconductor Materials*. New York, NY, USA: Wiley, 2001, pp. 1–30.

[25] M. Suzuki and T. Uenoyama, "First-principles calculation of effective mass parameters of gallium nitride," *Jpn. J. Appl. Phys.*, vol. 34, nos. 1–7, pp. 3442–3446, 1995.

[26] B. Santic, "On the hole effective mass and the free hole statistics in wurtzite GaN," *Semicond. Sci. Technol.*, vol. 18, no. 4, pp. 219–224, 2003.

[27] F. Römer and B. Witzigmann, "Acceptor impurity activation in III-nitride light emitting diodes," *Appl. Phys. Lett.*, vol. 106, no. 2, 2015, Art. no. 021107.
[28] K. Sakowski, L. Marcinkowski, S. Krukowski, S. Grzanka, and E. Litwin-Staszewska, "Simulation of trap-assisted tunneling effect on characteristics of gallium nitride diodes," *J. Appl. Phys.*, vol. 111, no. 12, 2012, Art. no. 123115.
[29] F. Schwierz, "An electron mobility model for wurtzite GaN," *Solid-State Electron.*, vol. 49, no. 6, pp. 889–895, 2005.
[30] J. Piprek, *Nitride Semiconductor Devices*. Weinheim, Germany: Wiley, 2010, pp. 69–93.
[31] T. T. Mnatsakanov *et al.*, "Carrier mobility model for GaN," *Solid-State Electron.*, vol. 47, no. 1, pp. 111–115, 2003.
[32] B. J. Baliga, "Gallium nitride devices for power electronic applications," *Semicond. Sci. Technol.*, vol. 28, no. 7, 2013, Art. no. 074011.
[33] R. Khanna, S. J. Pearton, F. Ren, and I. I. Kravchenko, "Stability of Ti/Al/ZrB 2/Ti/Au ohmic contacts on n-GaN," *Appl. Surface Sci.*, vol. 253, no. 4, pp. 2340–2344, 2006.
[34] Y.-J. Lin, "Electrical properties of Ni/Au and Au contacts on p-type GaN," *J. Vacuum Sci. Technol. B Microelectron. Nanometer Struct.*, vol. 23, no. 1, p. 48, 2005.
[35] B. Baliga, *Fundamentals of Power Semiconductor Devices*. New York, NY, USA: Springer, 2008, pp. 91–166.
[36] J. F. Ziegler, M. D. Ziegler, and J. P. Biersack, "SRIM—The stopping and range of ions in matter (2010)," *Nucl. Instrum. Methods Phys. Res. B Beam Interact. Mater. Atoms*, vol. 268, nos. 11–12, pp. 1818–1823, 2010.
[37] R. Perez *et al.*, "Planar edge termination design and technology considerations for 1.7-kV 4H-SiC PiN diodes," *IEEE Trans. Electron Devices*, vol. 52, no. 10, pp. 2309–2316, Oct. 2005.

MOHAMMED SHURRAB received the B.Sc. degree in electrical and electronic engineering from the Khalifa University of Science and Technology, Abu Dhabi, UAE, where he is currently pursuing the M.Sc. degree in electrical and computer engineering. His research interests include the design, modeling, and characterization of semiconductor devices and circuits for high-power, high-temperature, and high-speed applications.

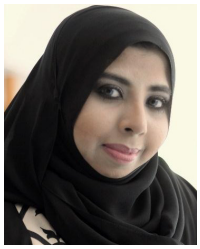

AMNA SIDDIQUI received the M.Sc. degree in electrical and computer engineering from the Khalifa University of Science and Technology, Abu Dhabi, UAE. Her research interests include designing and modeling novel devices and circuits for high temperature applications, wide bandgap semiconductor power devices, and small-sized digital integrated circuits for harsh environments.

SHAKTI SINGH received the B.Sc., M.Sc., and Ph.D. degrees in electrical and computer engineering from Purdue University, West Lafayette, IN, USA. He is currently an Assistant Professor with the Electrical and Computer Engineering Department, Khalifa University of Science and Technology, Abu Dhabi, UAE. His research interests include design, modeling, fabrication and characterization of semiconductor devices and integrated circuits with focus on wide band-gap semiconductors, power devices, and integrated circuits for high-power, high-temperature, and high-speed applications. His current work also includes sensors, sensing technologies, crowd sourcing, crowd sensing, and development of wireless and IoT-based sensor networks.